Environ Earth Sci (2016)75:650
DOI 10.1007/s12665-016-5481-0

ORIGINAL ARTICLE

Causes and processes of sandy desertification in Guinan County, Qinghai–Tibet Plateau

Xiaoying Li[1] · Zhengyi Yao[1] · Zhibao Dong[1] · Jianhua Xiao[1]

Received: 27 August 2015 / Accepted: 18 February 2016

Abstract By means of field investigations, interpretation of remote sensing images, analysis of a digital elevation model, and grain-size tests, we analyzed the causes and processes responsible for sandy desertification in Guinan County, on the Qinghai–Tibet Plateau. The desertified land is mainly distributed on the Mugetan region and covered 566 km^2, about 96.1 % of which distributed on the sandy hills. We found that reactivation of the underlying fossil dunes supplied the sand that contributed to modern sandy desertification. The surface turf, which supports a dense growth of grass and its matted roots, covers the underlying cohesive silty sands in the sandy hills, and both layers protect the dunes against erosion. Mechanical destruction of the protective shell leads to exposure of fossil dune sands. The exposed loose fossil sands are then carried away by the wind, creating scarps, followed by lateral recession at the bottom of the scarp, leading to its collapse. The process then repeats. With the expansion of recession caused by wind erosion, abundant sands are supplied and aeolian activity intensifies. Repetition of this process expands the blowouts, leading to merger of the blowouts and the evolution of mobile dunes. Similar processes occur at the top of cliffs above the Yellow River and Mangla River.

Keywords Sandy desertification · Mobile dunes · Reactivation of fossil dunes · Blowouts

✉ Zhengyi Yao
yaozy@lzb.ac.cn

[1] Key Laboratory of Desert and Desertification, Cold and Arid Regions Environmental and Engineering Research Institute, Chinese Academy of Sciences, 320 Donggang West Road, Lanzhou 730000, China

Introduction

The Qinghai–Tibet Plateau has experienced serious environmental problems and environmental changes for several millennia owing to its location at high elevations in a cold and semi-arid region of China (Hanvey et al. 1991; Xue et al. 2009). As a result of a warming trend in recent years, desertification, wetland shrinkage, permafrost degradation, and grassland degradation have become increasingly serious problems, and have received widespread attention (Tong and Wu 1996; Zhou et al. 2005; Avni et al. 2006; Xue et al. 2009; Li et al. 2015). Severe desertification has occurred in the Qaidam Basin, Gonghe Basin, the source regions of the Yellow River and Yangtze River, and along the middle reaches of the Yarlung Zangbo River and its two main tributaries (the Lhasa River and the Nyangqu River), as well as in the Ali region of the Qinghai–Tibet Plateau. Some research has suggested that the Qinghai–Tibet Plateau will experience increasing desertification and become an important dust source in China (Fang et al. 2004; Bai et al. 2006; Han et al. 2009b).

Guinan County, which lies in the Gonghe Basin (Fig. 1), is also undergoing desertification. The desertified land in Guinan is mainly distributed in the Mugetan region, an alluvial plain of the Yellow River that underwent uplift by tectonic movement at the end of the Middle Pleistocene. The Mugetan dune field is the largest continuous sand dune system in the Gonghe Basin; it is about 42 km long and 20 km wide, and covers 544 km^2. The surface soil in these regions overlies widely distributed fossil dunes and ancient sediments (Dong et al. 1993). Reactivation of these fossil dunes and ancient sediments has provided a large sediment source to support modern sandy desertification (Sun et al. 1998; Buynevich et al. 2007). In many other areas, such as Canada, the Arab regions, and northern China, modern sandy

Published online: 11 April 2016

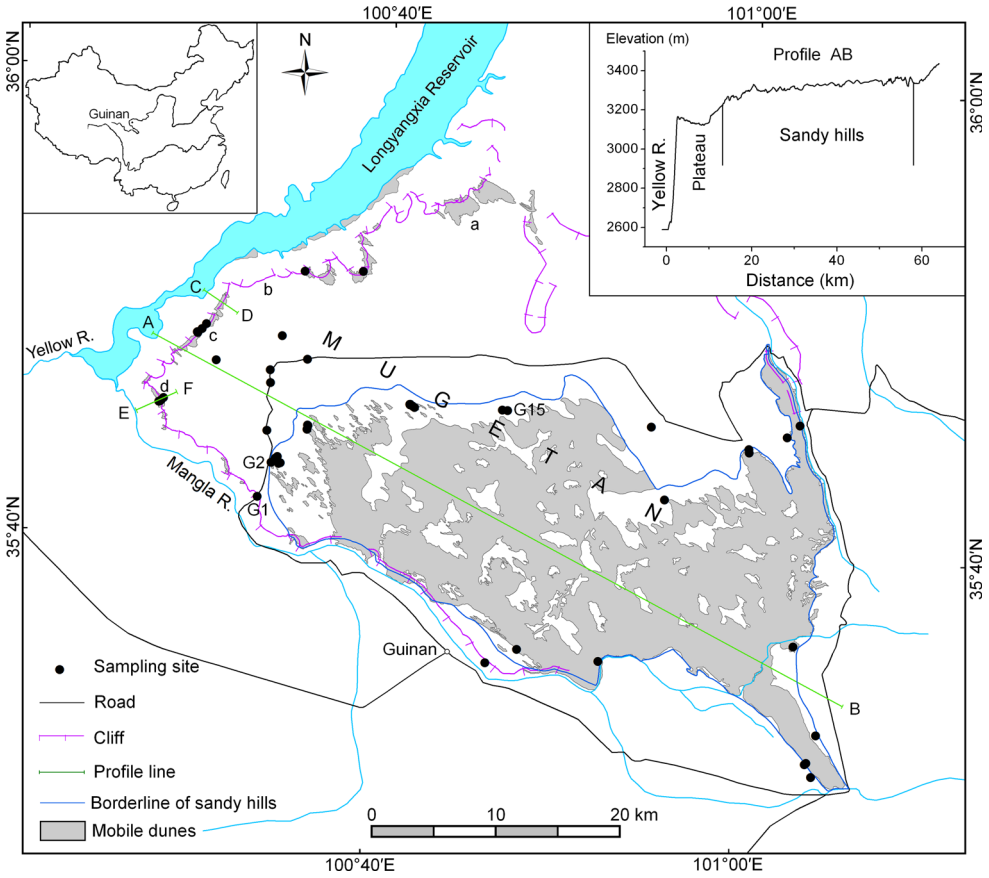

Fig. 1 Location of the study area and map of sandy desertification (source: 30 July 2013 Landsat 8 OLA_TARS satellite remote sensing image). The *inset* elevation profile represents the transect indicated by the line running southeast from point *A* to point *B*. *A* to *F* represent different transects shown in subsequent figures; *a* to *d* represent specific sites described in the text

desertification has also derived from the reactivation of fossil dunes, and the reactivation process has been well documented (Abahussain et al. 2002; Wang et al. 2002; Hugenholtz and Wolfe 2005). However, it is not yet clear how this reactivation has occurred in the Gonghe Basin. Previous work suggests that desertification in the Guinan region began ca. 2.0 Ma B.P., in the early Pleistocene (Dong et al. 1993). However, due to periodic climate change, desertification has advanced and receded alternately. The stratigraphic assemblage suggests that desertification has become increasingly frequent, with increasingly short periods between reversals, since the early Pleistocene (Dong et al. 1993). Based on the age estimates, Dong et al. proposed that the youngest paleosol (grayish-black silty sand) that underlies the modern dunes was deposited and buried 112 ± 57 a B.P. This suggests that the modern aeolian sandy sediments gradually developed after the 1840s (Dong et al. 1993). Previous scholars (Yang et al. 2005; Zhang et al. 2005) have proposed explanations of the driving forces for desertification in the Gonghe Basin. However, these driving forces, whether natural factors (cold, dry, and windy weather, combined with a rich supply of sandy materials and sparse and short vegetation) or human factors (over reclamation for agriculture, overgrazing, excessive cutting of fuelwood), cannot explain the characteristics of the mobile dunes described earlier in this section. For example, the weather characteristics do not vary greatly within the study area, yet there are areas of stable vegetation-covered sands adjacent to areas of mobile sands, and many areas have evolved into mobile dunes without high levels of anthropogenic impacts.

In the present study, we examined the distribution and characteristics of mobile dunes in Guinan County, as well as the stratigraphic structures and grain-size characteristics of the main sediments based on interpretation of remote sensing satellite images and detailed field investigations. Our main purpose was to elucidate the formation and development processes that lead to sandy desertification, including the influence of topography and the surface strata, thereby providing insights into the driving factors that control the distribution of desertified areas. The results also give reference significance to other desertified areas that derived from the fossil sands in Qinghai–Tibet Plateau and other countries.

Study area

Guinan is located in the northeastern Qinghai–Tibet Plateau, between the Qinghainanshan Mountains and the Ela Mountains, which form the borders of the Gonghe Basin

(Feng et al. 2008; Han et al. 2009a). This area is located in a transitional bioclimatic subzone between the plateau's temperate semi-arid steppes and desert steppes. The mean annual temperature from 1961 to 2007 was 2.4 °C, and the mean monthly temperature ranges from 13.2 °C in August to −11.5 °C in January. The lowest temperature recorded was −32.3 °C in 1956. Guinan County has experienced rising temperatures between 1961 and 2007, at a rate of 0.230 °C per decade (Guo et al. 2009), which is much higher than the mean value for China (0.044 °C per decade). However, the temperature has increased more rapidly from 1988 to 2007, at a rate of 0.393 °C per decade. As a result of these trends, the mean annual temperature increased from 2.1 °C between 1961 and 1987 to 2.7 °C after this period. (Yang et al. 2004; Hu et al. 2012; Sun et al. 2012). The mean annual temperature increased further, to 2.8 °C, from 2008 to 2014.

Annual average precipitation is 413 mm, and is concentrated in the period from June to August; 70 % of the total falls during this period. Based on data from the Guinan meteorological station, we calculate that precipitation has generally increased between 1957 and 2012, at a rate of 10.5 mm per decade. However, annual precipitation is characterized by high variability, with relative variation values in a given year ranging from −39.9 to 50.0 % of the long-term mean. Potential evaporation is far in excess of precipitation, even in a rainy year. The total annual potential evaporation is 1558.2 mm, which is 3.8 times the annual precipitation. Spring is the driest season, with potential evaporation of 537.9 mm and precipitation of only 74.3 mm, and the aridity index (potential evaporation divided by precipitation) is 7.2 (Dong et al. 1993).

The annual average wind speed is 2.5 m s^{-1}, with an average of 15.5 windy days, which we defined as days with a wind speed ≥17.2 m s^{-1} (Guo et al. 2009). Strong winds are concentrated in the spring, accounting for about 49.7 % of the windy days (Dong et al. 1989). The prevailing wind direction is from the northwest, with a frequency of 30 % (Fig. 2). The maximum wind speed exceeded 20 m s^{-1}. The cold and dry climate leaves the surface materials in a dry and loose state, which makes them vulnerable to erosion by the frequently strong wind.

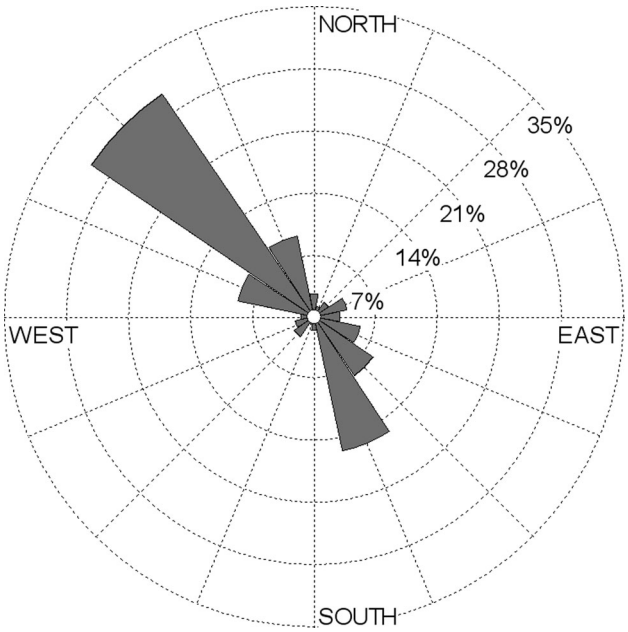

Fig. 2 Wind rose for the sand-entraining winds in the study area

Study methods

Field surveys were conducted in August 2014 and February 2015. A total of 47 sites were investigated to determine the stratigraphy, landforms, vegetation, and presence and characteristics of blowouts. Stratigraphy was examined in road cuts, blowouts, and in ditches. At each site, sediment samples were collected to determine the grain size using sieves with sizes defined using the Φ scale. The grain-size distribution characteristics were calculated using the equations and procedures of Folk and Ward (1957). The location of each site was determined using a portable global positioning system (GPS) receiver (Garmin eTrex Vista C; Garmin International, Olathe, KS, USA) with a horizontal accuracy of 4 m. The geometrical features of blowouts were measured using differential GPS (S82-C, SOUTH, Guangzhou, China), with a horizontal accuracy of 1.5 m.

Meteorological data, including precipitation, temperature, and wind velocity, were collected from the Climatic Data Center of the China Meteorological Administration's National Meteorological Information Center (http://www.nsmc.cma.gov.cn). Because the time span for the available wind direction data was short, we used data from only 5 years (2008–2012) to calculate the wind rose at the Guinan Meteorological Station.

The area of desertification was visually interpreted from a satellite remote sensing image obtained on 30 July 2013 (Landsat 8 OLA_TARS). The migration rates of mobile dunes were determined by comparing satellite images from different periods (9 September 1987, Landsat 4–5TM; 30 July 2013, Landsat 8 OLA_TARS). A digital elevation models (DEM) with 90-m spatial resolution and fine-resolution Google Earth (https://www.google.com/earth/) images were used to determine the boundary of the area of sandy hills. The DEM and satellite remote sensing images were obtained from China's Geospatial Cloud (http://www.gscloud.cn).

Results

Landforms and the distribution of mobile dunes

The primary type of sandy desertification in Guinan is mobile dunes. Based on a satellite remote sensing image from 30 July 2013 (Landsat 8 OLA_TARS), the mobile dunes in Guinan cover 566 km^2 (Fig. 1), mainly in the Mugetan region. The Mugetan dune field accounts for 96.1 % of the total area of mobile dunes in Guinan. Part of the dune field extends along the Yellow River and Mangla River cliffs in the northwestern and southwestern parts of the study area, respectively. These dune fields show discrete bands that together cover an area of 16 km^2. Other dune fields are distributed beside the water, at elevations of 2580–2630 m, on the eastern shore of the Longyangxia Reservoir, and some are found in gullies at the northern edge of Mugetan, where they together cover an area of 7 km^2. These patches of mobile dunes are greatly influenced by changes in the reservoir's water level. However, the formation mechanism of these small areas of mobile dunes is beyond the scope of this paper.

Mugetan lies in the Yellow River's alluvial plain, which slopes gently downward towards the northwest (inset graph in Fig. 1), with the elevation decreasing from 3500 to 3100 m over a distance of 50 km. However, inside the Mugetan area, the local topography is complex. The landscape is composed of plains and uplands with undulating terrain, alternating between plateau areas and sandy hills. The plateau areas are relatively flat terrain, with an elevation ranging from 3130 to 3300 m. They are primarily distributed in a half ring shape at the northwestern side of Mugetan, and have been partly cultivated as farmland and artificial grassland. Apart from small areas at the northwestern and southern sides of the plateau, there are no mobile dunes in the plateau regions.

Sandy hills lie close to the central and southeastern parts of Mugetan, with elevations of around 3200 m (western side) and more than 3300 m (northern side), at elevations 20–60 m higher than the adjacent plateau areas. The area is characterized by large, parallel fossil dune ridges that are currently covered by herbaceous vegetation, with a vegetation cover of at least 40 % throughout most of the area (see "Formation process for the mobile dunes" for details). Blowouts have developed in many of the elongated sand ridges. The mobile dunes (severely desertified land) and grassland (non-desertified land) form a mosaic in which the two cover types are contiguous, with no gradient between them. For example, many isolated bands of mobile dunes are scattered in grassland at the northwestern (upwind) side of the dune fields, and some of these bands have begun to merge with the dune fields. Meanwhile, in the Mugetan dune fields, dozens of patches of grassland (fixed dunes) scattered among the dunes.

Stratigraphy and grain characteristics

Field surveys show that the stratigraphy of the plateau and sandy hills are somewhat different. In the plateau areas, the uppermost layer is grayish-black or gray silty sand about 1.7–2.8 m thick. Under this layer lie fossil dune sands, with a maximum thickness of 11.5 m at the G1 site.

In the sandy hills, the uppermost layer is gray-yellow aeolian sand ranging from 0.2 to 2.0 m in thickness. The second layer is grayish-black or gray silty sand similar to that in the plateau and that formed at the same time, with a thickness generally ranging from 0.8 to 1.7 m. However, the thinnest layer is only 0.1 m. The third layer is a gray-yellow or gray fossil dune sand, with an unknown thickness because there are few naturally exposed sections or excavations by researchers. Only individual sites, such as the G15 site (35.76560°N, 100.78319°E, 3325 m a.s.l.) have exposed sequences. At this site, the fossil dune sand layer is 0.8 m thick. The fourth layer is 0.6 m thick and is well cemented grayish black silty sand. The fifth layer is a loose fossil dune sand, with a thickness of 2.0 m. Based on these results, Dong et al. (1993) suggested that the Mugetan stratigraphy is characterized by interbedded silty sands and fossil dune sands, and their deepest sequence included 10 layers, with the deepest section reaching 10 m in depth. The surface aeolian sands appear to have been derived from the layer of fossil dune sands during the most recent period of sandy desertification.

The silty sand layer on the plateau is thicker than that in the sandy hills, and is widely distributed. In most cultivated areas, the soil is only tilled to a depth of 0.4 m, which cannot reach the depth of the fossil dune sands. Some ditches that have been dug to a depth of 1.5–2 m on the plateau also do not expose the fossil dune sands. Although tilling has heavily disturbed the surface soil of the plateau, it has generally not produced desertification. However, the surface silty sand layer in the plateau is a significant source of dust when it is exposed (Fang et al. 2004). Repeated tillage, combined with wind erosion during periods with no crop cover, has decreased the silt content (Liu et al. 2003). When the silt content is less than a certain value (about 15 % in the study area by analyzing silt content and cemented condition of all the samples), the silty sands will lose cohesion and sand mobility will increase.

Table 1 summarizes the grain-size distribution characteristics based on 84 sediment samples from 47 sites in the Mugetan region. Figure 3 shows the frequency curves for the grain-size distributions of the sediment samples from eight representative stratigraphic sequences.

Table 1 Grain-size parameters based on 84 samples from the Guinan County study area

Site type	Sample type	Very coarse sand 2–1 mm	Coarse sand 1–0.5 mm	Medium sand 0.5–0.25 mm	Fine sand 0.25–0.125 mm	Very fine sand 0.125–0.063 mm	Coarse silt 0.063–0.0315 mm	Medium silt <0.0315 mm	Mean size (Mz, Φ units)	Standard deviation (σ, Φ units)
Plateau	Mobile dune sands ($n = 6$)	0.57	1.87	18.97	62.68	14.28	1.61	0.01	2.42	0.61
	Surface aeolian sands ($n = 5$)	–	0.33	8.54	45.57	33.87	10.97	0.71	3.01	0.73
	Silty sands ($n = 21$)	–	0.06	0.75	15.98	50.93	30.51	1.77	3.71	0.57
	Fossil dune sands ($n = 11$)	–	0.02	1.66	40.44	46.44	11.00	0.43	3.22	0.61
Sandy hills	Mobile dune sands ($n = 5$)	–	0.03	3.83	82.54	13.15	0.45	–	2.63	0.35
	Surface aeolian sands ($n = 9$)	–	0.05	2.86	49.09	40.47	7.04	0.48	3.08	0.57
	Silty sands ($n = 13$)	–	–	0.48	26.01	40.39	32.69	0.43	3.55	0.62
	Fossil dune sands ($n = 14$)	0.03	0.24	3.61	50.34	42.11	3.53	0.13	3.00	0.53

Although there are some differences between the silty sands from the plateau and sandy hills, both are dominated by very fine sands and coarse silt (0.125–0.0315 mm), amounting to 81.4 and 73.1 % of the total, respectively, indicating that these sediments collected dust during a period of desertification reversal. However, the fine sand content in the sandy hills is much higher (by 3.4–20.2 percentage points) than that on the plateau for the corresponding soil types. Coarse silt and some of the very fine sands serve as dust sources, and would have been blown away by the wind in the plateau areas.

The grain-size distribution shows high similarity among the mobile dune sands, surface aeolian sands, and fossil dune sands in the sandy hills. All of these sediments are dominated by fine and very fine sands (0.25–0.063 mm), which account for 95.7, 89.6, and 92.4 % of the total, respectively.

The grain-size distributions of the surface aeolian sands and fossil dune sands in the plateau are similar. However, the content of medium sands (19.0 %) in the mobile dune sands at the edges of the plateau is much higher than that of the sandy hills (3.8 %), partly due to a supply of coarse and medium sands from the sandy gravel layer.

Compared with the fossil dune sands described in the previous paragraph, the mobile dune sands have a greatly increased fine sand content (by 22.2 % points on the plateau versus 32.2 % points in the sandy hills) and a greatly decreased very fine sand content (by 34.2 % points on the plateau and by 29.0 % points in the sandy hills), with a coarser mean size. The sandy materials of the mobile dune sands appear to be derived from the fossil dune sands, although changed somewhat by the wind action. However, coarse sands that come from sandy gravel of the cliffs would contribute to the mobile dune sands. Therefore, coarse grain of mobile sands in the plateau is more than that of in the sandy hills.

Formation process for the mobile dunes

Because Guinan is located in the temperate semi-arid steppe region of China (Institute of Geography 1999), the land is characterized by sparse vegetation with a coverage ranging from 40 to 80 %. Most of the plants are grassland species, such as *Achnatherum splendens*, *Orinus thoroldii*, *Agropyron cristatum*, *Stipa* spp., *Peganum harmala*, and *Caragana sinica*, with a height ranging from 10 to 40 cm (Dong et al. 1993). The root systems of these grasses reach a depth of 50–80 cm (Luo et al. 1999). According to our field surveys, the densest roots are concentrated in the top 20 cm of the soil. These dense roots bind the soil particles tightly together to form a thick turf. The mechanical strength of the turf is greater than that of similar soil without root systems, and can protect the underlying loose

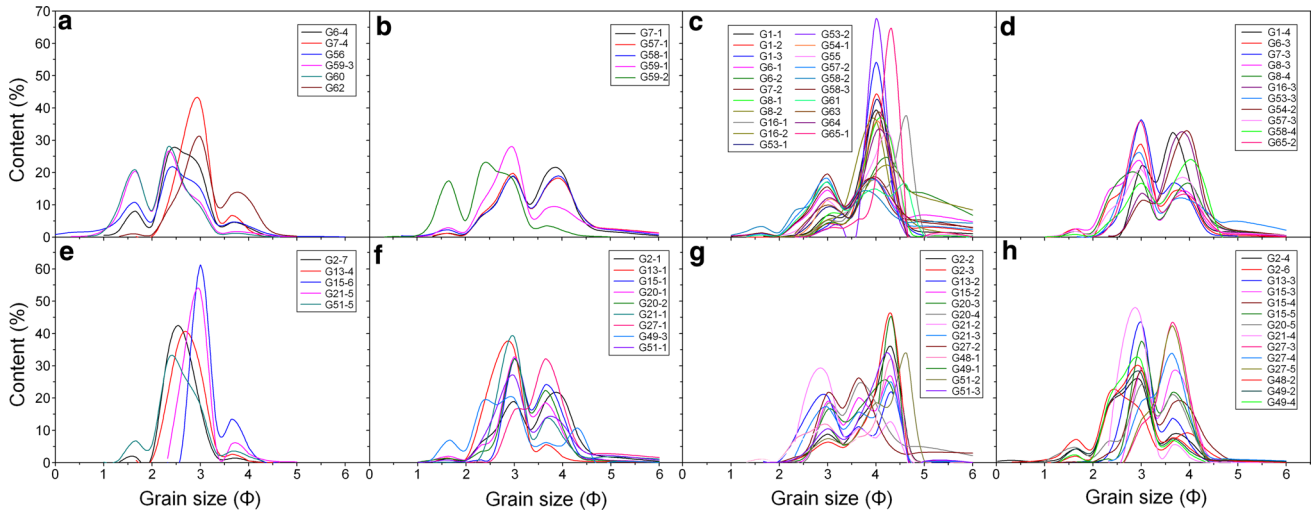

Fig. 3 Grain-size distributions for the samples in Table 1, *lines* with *different colors* represent the 84 samples from the 47 sample sites. For the plateau areas: **a** mobile dune sands, **b** surface aeolian sands, **c** silty sands, **d** fossil dune sands. For the sandy hills: **e** mobile dune sands, **f** surface aeolian sands, **g** silty sands, **h** fossil dune sands. *Letters* correspond to the sample locations shown in Fig. 1

sediments from wind erosion. In addition, the widely distributed silty sands in the Mugetan region are well cemented and have good mechanical strength. Therefore, they resist erosion by the wind, and offer good protection to the underlying loose sands. The combination of the turf and the silty sands provides good protection for the underlying loose sands. However, if this protective shell is destroyed, the underlying loose sands are exposed and are easily eroded by the region's frequently strong winds. This appears to be the main reason for the formation of mobile dunes in the Mugetan region. However, various processes occur that expose the loose sands and permit the development of mobile dunes.

Formation of blowouts in the sandy hills

Based on the field surveys and analysis of high-resolution satellite images, we found that many isolated narrow strips of mobile dunes had developed on the western and northwestern sides of the dune field. Extension and connection of these dunes have resulted in the formation of large and continuous mobile dunes. Analysis of the formation and development processes that create the smaller, isolated mobile dunes will contribute to our understanding of the formation of the larger, continuous mobile dunes.

For example, we found a blowout at the G2 site (35.72153°N, 100.57090°E, 3207 m a.s.l.). The blowout is 325 m long, has a maximum width of 115 m and maximum depth of 27 m, and has a strike of 111° (southeast). The deepest part is located at the northwestern bottom of the blowout, and the depth decreases towards the southeast. The western and northern sides of the blowout have a 2.2-m-tall scarp. The strata of the scarp (Fig. 4, insets) reveal an aeolian sand with a thickness of 0.4 m at the surface, silty sands with a thickness of 2.0 m in the middle, and a relatively loose fossil dune sand of unknown thickness as the bottom layer (Fig. 4).

Field surveys indicated that loose sand at the bottom of the scarp is blown away by the wind, undercutting the bottom soil to a depth of up to 20 cm. Next, vertical joints develop in the silty sand layer above the undercut, and some of the joints open, creating a tendency for the surface to collapse. The collapsed soil mass slides partway down the slope, and accumulates at the foot of the scarp. The accumulation wholly or partly covers the loose sand that has already been exposed, and provides some protection. However, the collapsed mass would be eroded and carried away by wind, exposing the loose sand layer, which is then vulnerable to undercutting. Repetition of these steps would both lead to growth of the blowout and provide a growing supply of sandy material for transport by the wind.

However, this description does not explain how the blowout originally formed. Based on the field surveys and high-resolution satellite images, we found many bands of ridges that had developed in the sandy hills. The ridges are 10–40 m high, 40–100 m wide, and 700–900 m long. Their strikes range between 120° and 140° (i.e., downwind towards the southeast). These ridges are asymmetric, with a steeper slope on the northeastern side (19.7°–35.2°) and a relatively gentle slope (8.5°–16.6°) on the southwestern side.

Silty sands on the sandy hills vary greatly in their thickness, with the thinnest layer only 10 cm thick (e.g., Fig. 5a). The thinnest layers are most easily damaged by trampling, creating shallow grooves in the sandy hills (Fig. 5b). Our field surveys showed that the shallow

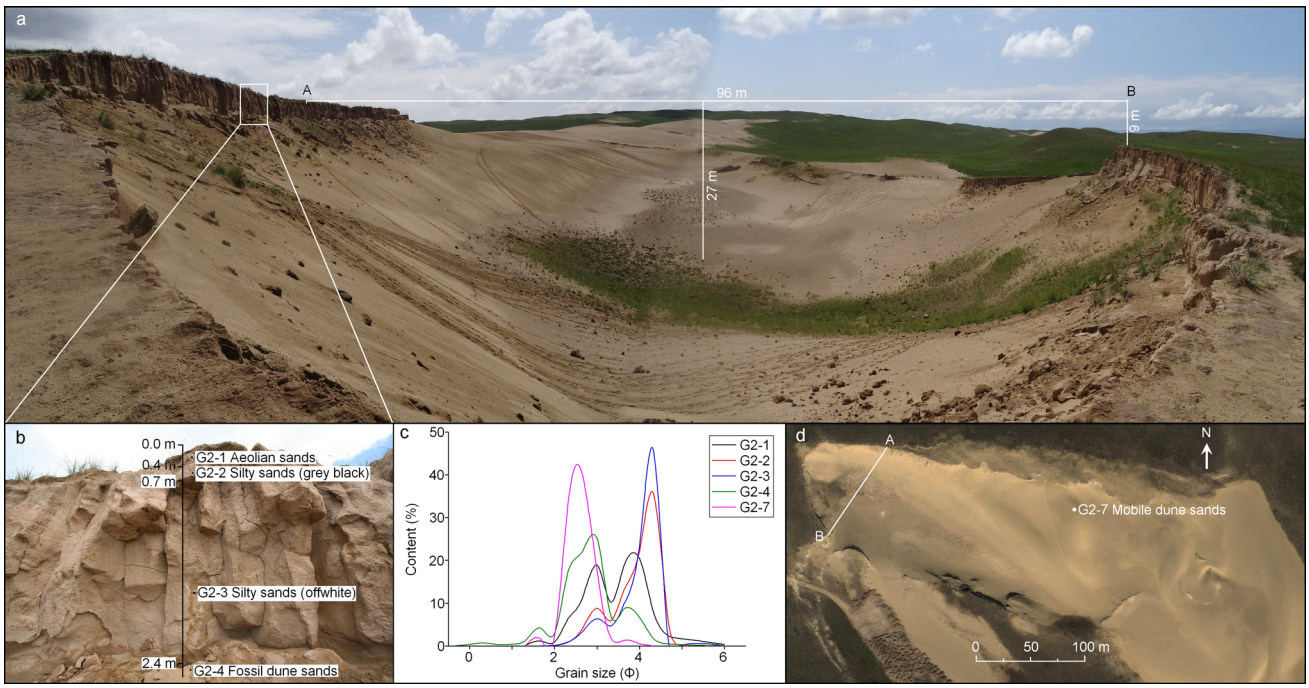

Fig. 4 An example of a large blowout (the G2 site in Fig. 1) that provides a source of sand for the surrounding area. **a** Overview of the blowout. **b** Stratigraphy and sampling position. **c** Grain-size frequency curves for the samples from **b** and **d**. **d** Satellite photograph of the blowout. The *line* from *A* to *B* represents the cross section shown in **a**

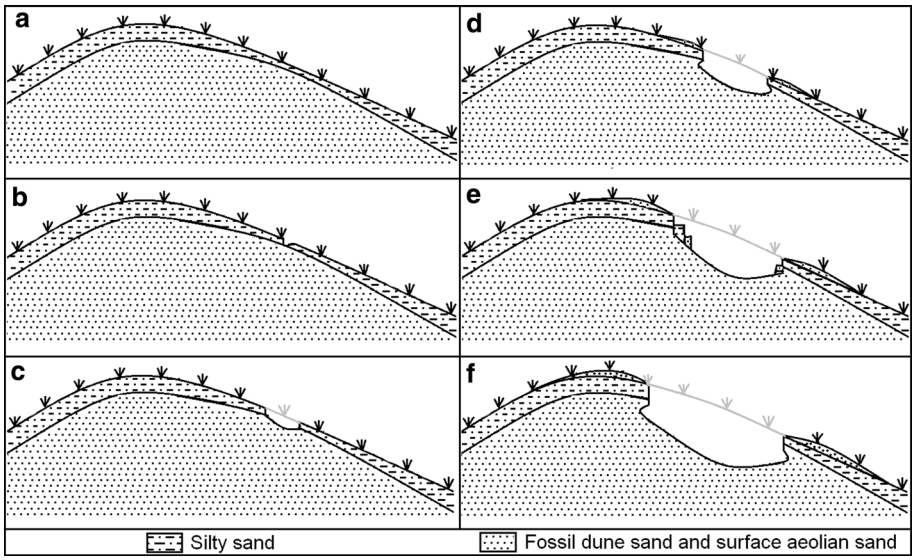

Fig. 5 Illustration of how blowouts develop in the sandy hills. **a** In stage 1, the process begins with an asymmetric ridge with a significant difference in the thickness of silty sands. **b** In stage 2, trampling by livestock creates shallow grooves, particularly in areas with a thinner turf and silty sand layer. **c** In stage 3, fossil dune sands are exposed and eroded by the wind, forming a small blowout. **d** In stage 4, scarps form, exposing the loose fossil sands, which are then removed by the wind, creating lateral recession (undercutting) at the bottom of the scarps. **e** In stage 5, the upper silty sands collapse, providing cover for the loose sands. **f** In stage 6, the collapsed materials are eroded and carried away, and the loose sands are exposed to erosion again

grooves were about 15 cm deep with a width of about 20 cm. Repeated trampling by livestock exposes the fossil dune sands, which are then eroded by the wind, forming a small blowout (Fig. 5c). The blowouts have developed on the slopes and at the top of the ridges, particularly on the southeastern slope. Most of the blowouts are elliptical, with a long axis of 13–59 m, a short axis of 10–25 m, and a depth of 3–5 m. Blowouts are dish-shaped, with the

deepest part at the center. At the brink of the blowouts, slump scarps form. Formation of the scarps strengthens the wind at the bottom of the scarp, increasing its erosive power. Loose fossil sands are then removed by the wind, creating lateral recession at the bottom of the scarp (Fig. 5d). When the depth of the lateral recession is sufficiently large, the upper silty sands collapse (Fig. 5e), and the accumulated mass wholly or partly covers the loose sand that has already been exposed, providing some cover for the loose sand. However, with the passage of time, the collapsed materials are eroded and carried away by wind, rain, and gravity, and the loose sand is exposed again (Fig. 5f). Repetition of these processes leads to expansion of the blowouts. Some of the larger blowouts can reach 90–130 m in length, with a depth of about 10–20 m. Connection of adjacent blowouts leads eventually to the formation of mobile dunes.

Enlargement of a blowout is a slow but intense process. Its rate of growth is related primarily to wind erosion (although heavy rain is another possible factor), but other natural and human factors do not appear to accelerate the process in our study area. That is, we found no evidence of cultivation or wood harvesting where blowouts had occurred. The formation of scarps also provides an ideal place for burrowing rodents, which may dig burrows in the scarp. The scarps sometimes attract cattle and sheep, which use the sharp edges to scratch their itches. Such activities accelerate the retreat of the scarp. However, we have no data on the effects of these additional processes.

From the perspective of wind erosion, the effect depends on the direction of the wind relative to the scarp. When the wind direction is parallel to the scarp or strikes the scarp at an acute angle, the deposits formed by falling sediments can be blown away by the wind, leading to rapid exposure of the underlying loose sand. However, when the wind direction is more perpendicular to the scarp, the blown sand will accumulate at the location of the collapse, providing a protective cover for the loose sand.

By comparing the satellite images from different periods, we calculated that mobile dunes in the Mugetan region are moving southeast at a rate of 2.3 m year^{-1}, and will finally encroach on some downwind grassland areas. In some places, the sandy materials slide over steep cliffs and hillsides, where they form falling dunes. Therefore, this is another way in which desertification expands in the Mugetan region.

River terraces and cliffs

Due to the strong incision produced by the Yellow River and its tributary, the Mangla River, steep cliffs have developed at the northwestern and southern edges of the Mugetan region, with a height of 300–500 m (Fig. 1, inset graph). The slope of the cliffs ranges between 30° and 32°. Generally, the slopes are covered with eroded material, including silty sands and fossil dune sands. Initially, there is sufficient vegetation cover on the cliff face that most parts of the slopes have no erosion. Our geological surveys have revealed several layers of fossil dune sands and silty sands in the cliff strata. These strata are exposed on steeper slopes, but are covered with eroded material on gentler slopes.

The formation of the modern mobile dunes at the edges of the cliffs appears to have followed the same processes that formed the dunes in the sandy hills. Figure 6 illustrates the main stages of scarp development in the cliffs. Figure 6a shows the initial status of the cliff, covered with vegetation. The vegetation protects the sediments against wind erosion, and aeolian activity therefore does not take place. However, due to topographic effects, winds accelerate at the top of the slope. If the surface vegetation is damaged sufficiently, this can lead to strong wind erosion by the accelerated wind. As a result of a combination of water erosion and wind erosion, a depression may develop on the slope of the cliffs, as shown in Fig. 6b. The surface vegetation disappears from this depression, and under the influence of strong western and northwestern winds, the fossil dune sands begin to erode, forming a lateral undercut (recession), as shown in Fig. 6c. The top layer of silty sands collapses and accumulates at the bottom of the newly formed scarp, where it partly or wholly covers the fossil dune sands, as shown in Fig. 6d. At the same time, the wind starts depositing a thin cover of sandy materials at the top of the cliffs by transporting eroded materials upwards from the bottom of the scarp and from other lower positions on the slope. Currently, this sand accumulation at the top of the scarp can be observed in many places. Subsequently, as shown in Fig. 6e, the accumulated mass of eroded materials is carried away by wind and water, exposing the fossil dune sands again and leading to additional erosion. Repetition of these processes destroys the surface protective shell and leads to reactivation of the fossil dunes, culminating in the formation of the modern mobile dunes.

However, some of the areas at the top of the cliffs have no mobile dunes, or have dunes that are highly variable in size. In places with large V-shaped gullies, the wind is strongly accelerated by topographic effects, leading to the development of wide dunes that can reach lengths of up to 1.9 km (e.g., Fig. 1, position “a”). However, at locations with smaller gullies, due to the weaker wind acceleration, there are either no dunes or narrow dunes, and the maximum dune length is only 0.8 km (e.g., Fig. 1, locations “b” and “c”). On the cliffs northeast of the Mangla River, weak winds, with a small proportion coming from the southwest, have created a small dune area (Fig. 1, location “d”). On

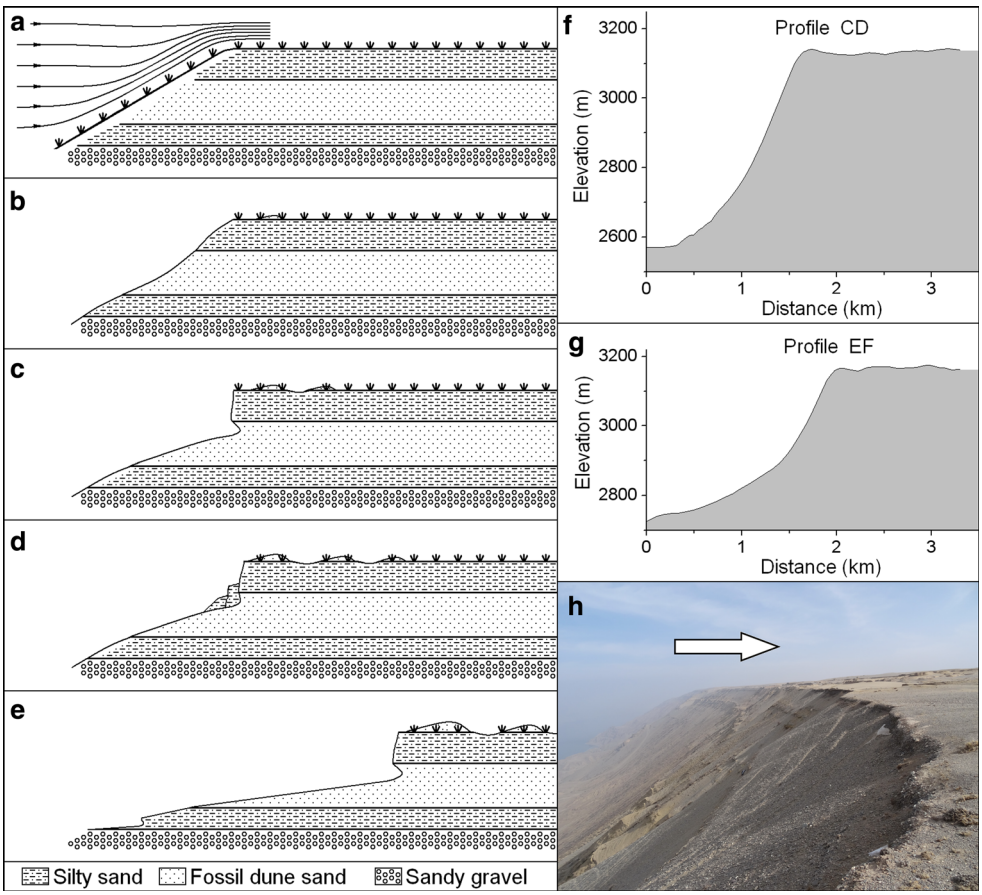

Fig. 6 Model of the erosion and deposition processes that occur at the top of cliffs created as a result of incision by the area's main rivers (Fig. 1). **a** In stage 1, the cliff is covered with vegetation that protects it against wind and water erosion. However, wind accelerated by topographic effects creates stronger winds at the top of the slope. **b** In stage 2, wind and water erosion destroy the surface vegetation. **c** In stage 3, the fossil dune sands are exposed and a lateral undercut (recession) is created by wind erosion. **d** In stage 4, the top layer of silty sands collapses and accumulates at the bottom of the newly formed scarp, where it partly or wholly covers the loose fossil sands. **e** In stage 5, the accumulated mass of materials are eroded and carried away, and the fossil dune sands are exposed and begin to sustain erosion again. **f** Profile of the cliffs above the Yellow River along the transect from positions *C* to *D* (Fig. 1). **g** Profile of the cliffs above the Mangla River along the transect from positions *E* to *F* (Fig. 1). **h** Photograph of the cliffs above the Yellow River. The *arrow* shows the prevailing wind direction

the cliffs above the Longyangxia Reservoir, our analysis of satellite images from different periods suggests that the dunes have migrated southeast at 7.3 m year^{-1}, which is 3.2 times the rate we observed in the sandy hills. The migration rate of mobile dunes on the cliffs above the Mangla River is slower, at 2.3 m year^{-1}.

Discussion

In many countries, reactivation of fossil dunes or fixed dunes is common. Examples include Mali (Nickling and Wolfe 1994), South Africa (Bate and Ferguson 1996), New Zealand (Hesp 2001), the Arabian Peninsula (Bray and Stokes 2003), the Netherlands (Arens et al. 2004), Israel (Levin and Ben-Dor 2004), Canada (Hugenholtz and Wolfe 2005), Australia (Fitzsimmons et al. 2007), Patagonia (del Valle, et al. 2008), the United States (Girardi and Davis 2010; Barchyn and Hugenholtz 2013a; McKean et al. 2015), and Finland (Matthews and Seppälä 2014). In China, reactivation has been found in the Mu Us, Onqin Daga, Horqin, and Hulun Buir sandy lands (Sun and Ding 1998; Gao et al. 2001; Yang et al. 2007). Reactivation appears to be the main reason for the development of sandy desertification in these regions.

Many researchers have studied the mechanisms responsible for sandy desertification in Mugetan. However, the microscale causes and processes of sandy desertification are poorly understood. In particular, little is known about how reactivation of fossil dunes proceeds from a vegetated state in this area (Dong et al. 1993; Zhang et al. 2005). The spatial and temporal patterns of reactivation in

Mugetan provide some clues about potential causes. Not all of the dunes within the Mugetan area are reactivating, which suggests that the causes may be spatially variable. Some fossil dunes have been totally reactivated, and have now formed mobile dunes. Some are only partially reactivated, but are currently undergoing reactivation. Some remain intact, in their original states.

In general, dune reactivation can be driven by increased aridity, wind speed, fire, biogenic disturbance, human disturbance, or a combination of these factors (Barchyn and Hugenholtz 2013b). Our research results suggest that the drivers did not differ obviously, but that differences in the geometry and stratigraphy of the fossil dunes are responsible for the observed differences in reactivation. Because of the presence of silty sands in Guinan, well cemented silty sands and turf have developed, and both can act as a shell that protects the fossil dunes. However, the thickness of the silty sand varies widely, and blowouts appear to have been created in areas with the thinnest protective shell. On the other hand, the vegetation on the dunes varies somewhat. For example, the vegetation grows better on shady slopes than on sunny slopes. This is why the small blowouts appear to mainly exist on the southwestern side of the sandy ridges. Overgrazing may also be responsible for localized weakening of the protective vegetation.

Formation of a blowout is the key step for fossil dune reactivation, and disturbance is essential for blowout formation. In Guinan, we detected anthropogenic features in the satellite images that hinted at a link between reactivation and livestock disturbance. Livestock play a role by breaching the protective shell; thereby exposing the fossil sand to wind that can subsequently form blowouts. Vehicle tracks and digging by small animals such as marmots may also contribute to blowout development.

Barchyn and Hugenholtz (2013b) have defined a conceptual model of blowout expansion that is similar to the model we have proposed. In our model, we emphasized the action of lateral recession and gravitational collapse, creating erosion that leads to the expansion of blowouts. We also observed erosion by rain and biogenic disturbance (livestock scratching their itches, rodents digging), which would contribute to this process. Barchyn and Hugenholtz (2013b) studied colonization of the exposed soil by various species, and proposed that this process plays an important role in suppressing blowouts. In contrast to Barchyn and Hugenholtz, who observed colonizer species stabilizing the surface on the downwind side of blowouts, possibly due to transport of seeds, we observed colonization by plants on the slopes and at the bottom of the blowout. These species were not becoming established from seeds, but instead represented re-rooting of the surface vegetation on the collapsed sediments. This provides a clue for how to combat these blowouts: transplant plants with intact root systems to the exposed soil.

Conclusions

Previous research suggested that the driving forces responsible for the desertification in the Gonghe Basin (including the Guinan region) included natural factors (the cold, dry, and windy weather; a rich supply of sandy materials; sparse and short vegetation) and human factors (over reclamation of land for agriculture, overgrazing, vegetation removal). However, those hypotheses could not explain why mobile dunes (severely desertified land) and grassland (non-desertified land) formed a mosaic in which natural and degraded lands were contiguous, with no gradient between them. Our study, which combined field investigations with interpretation of remote sensing images, analysis of DEM data, and grain-size analyses, provided new insights into the mechanisms of desertification in Guinan County, and led us to propose a model that can explain the mosaic nature of the dunes and vegetated areas.

Our study showed that fossil dune sands appear to be the sources of the materials in the mobile dune sands; their grain-size distributions are similar, but with differences that can be explained by wind action during transport of the eroded particles. Reactivation of the fossil dunes appears to be the main reason for the development of sandy desertification. The thick turf in areas with high vegetation cover and the cohesive silty sand layer create a protective shell that shields fossil dunes from erosion by the wind. Mechanical destruction of the protective shell is the key step in initiating sandy desertification, since it leads to the development of slump scarps, which expose the fossil dune sands. Where loose fossil sands are exposed, they are eroded by the wind; forming lateral undercuts (recession) that causes the surface protective shell to collapse. As wind erosion expands these eroded areas, sand is supplied abundantly and aeolian activity intensifies. Repetition of these processes expands the blowouts, leading to connection of the blowouts and, finally, the formation of mobile dunes. A similar process occurs in cliff areas above the two main rivers in the study area.

These insights provide a deeper understanding of the mechanisms responsible for desertification in Guinan County, and should lead to better ways to prevent or mitigate desertification in this area. For example, protection of the turf and silt layers against damage could reduce the frequency of blowouts, and transplanting of rooted vegetation to protect exposed fossil sands from the wind could stabilize the sand and protect it against erosion.

Acknowledgments This work was funded by the Ministry of Science and Technology of the People's Republic of China (2013CB956000). The dataset used in our analysis was provided via the International Scientific & Technical Data Mirror Site, Computer Network Information Center, Chinese Academy of Sciences. (http://www.gscloud.cn). We thank Geoff Hart for editing the manuscript. We also thank the journal's anonymous reviewers and editor, whose insightful comments and suggestions were helpful in improving the quality of this paper.

References

Abahussain AA, Abdu AS, Al-Zubari WK, El-Deen NA, Abdul-Raheem M (2002) Desertification in the Arab region: analysis of current status and trends. J Arid Environ 51(4):521–545

Arens SM, Slings Q, De Vries CN (2004) Mobility of a remobilised parabolic dune in Kennemerland, The Netherlands. Geomorphology 59(1):175–188

Avni Y, Porat N, Plakht J, Avni G (2006) Geomorphic changes leading to natural desertification versus anthropogenic land conservation in an arid environment, the Negev Highlands, Israel. Geomorphology 82(3):177–200

Bai HZ, Ma ZF, Dong WJ, Li D, Fang F, Liu D (2006) Climatic properties and sandstorm causes in Tibet Plateau. J Desert Res 26(2):249–253 **(in Chinese with English summary)**

Barchyn TE, Hugenholtz CH (2013a) Dune field reactivation from blowouts: Sevier Desert, UT, USA. Aeolian Res 11:75–84

Barchyn TE, Hugenholtz CH (2013b) Reactivation of supply limited dune fields from blowouts: a conceptual framework for state characterization. Geomorphology 201:172–182

Bate G, Ferguson M (1996) Blowouts in coastal foredunes. Landsc Urban Plan 34(3):215–224

Bray HE, Stokes S (2003) Chronologies for late Quaternary barchan dune reactivation in the southeastern Arabian Peninsula. Quat Sci Rev 22(10–13):1027–1033

Buynevich I, Bitinas A, Pupienis D (2007) Reactivation of coastal dunes documented by subsurface imaging of the Great Dune Ridge, Lithuania. J Coast Res 50:226–230

del Valle HF, Rostagno CM, Coronato FR, Bouza PJ, Blanco PD (2008) Sand dune activity in north-eastern Patagonia. J Arid Environ 72(4):411–422

Dong GR, Gao SY, Jin J, Li BS, Zhou GC (1989) Land desertification and its control in Gonghe Basin, Qinghai Province. J Desert Re 9(1):61–71, 75 **(in Chinese with English summary)**

Dong GR, Gao SY, Jin J (1993) Land desertification and its remedial measures in the Gonghe Basin, Qinghai Province. Science Press, Beijing **(in Chinese with English summary)**

Fang XM, Han YX, Ma JH, Song LC, Yang SL, Zhang XY (2004) Dust characteristic and loess accumulation on the Tibetan Plateau—a case study of dust event on 4 March 2003 in Lhasa. Chin Sci Bull 49(9):953–960

Feng YM, Lu Q, Wang XQ, Yang HH, Sun DF (2008) Land desertification dynamic analysis based on remote sensing in Guinan County of Qinghai Province. Remote Sens Technol Appl 23(6):633–638 **(in Chinese with English summary)**

Fitzsimmons KE, Bowler JM, Rhodes EJ, Magee JM (2007) Relationships between desert dunes during the late Quaternary in the Lake Frome region, Strzelecki Desert, Australia. J Quat Sci 22(5):549–558

Folk RL, Ward WC (1957) Brazos river bar: a study in the signification of grain size parameters. J Sediment Petrol 27(1):3–26

Gao SY, Wang GY, Ha S, Su ZS (2001) A case study on desert evolution in the northwestern fringe of monsoon area, China since the last glacial epoch. Quat Sci 21(1):66–71 **(in Chinese with English summary)**

Girardi JD, Davis DM (2010) Parabolic dune reactivation and migration at Napeague, NY, USA: insights from aerial and GPR imagery. Geomorphology 114(4):530–541

Guo LY, Zhong C, Ding SX, Han HF (2009) Local climate changes and their impacts on grassland degradation in Gonghe Basin of Guinan County of Qinghai Province in past half-century. Chin J Agrometeorol 30(2):147–152 **(in Chinese with English summary)**

Han HH, Yang TB, Wang YL (2009a) Dynamic analysis of land use and landscape pattern changes in Guinan County, Qinghai, in the past 30 years. Progr Geogr 28(2):207–215 **(in Chinese with English summary)**

Han Y, Fang X, Zhao T, Bai H, Kang S, Song L (2009b) Suppression of precipitation by dust particles originated in the Tibetan Plateau. Atmos Environ 43(3):568–574

Hanvey PM, Dardis GF, Beckedahl HR (1991) Soil erosion on a subtropical coastal dune complex, Transkei, southern Africa. GeoJournal 23(1):41–48

Hesp PA (2001) The Manawatu dunefield: environmental change and human impacts. N Z Geogr 57(2):33–40

Hu GY, Dong ZB, Lu JF, Yan CZ, Wei ZH (2012) Land desertification and landscape pattern change in the source region of Yangtze River. J Desert Res 32(2):314–322 **(in Chinese with English summary)**

Hugenholtz CH, Wolfe SA (2005) Recent stabilization of active sand dunes on the Canadian prairies and relation to recent climate variations. Geomorphology 68(1):131–147

Institute of Geography, Chinese Academy of Sciences (1999) Atlas of the Tibet Plateau. Science Press, Beijing **(in Chinese)**

Levin N, Ben-Dor E (2004) Monitoring sand dune stabilization along the coastal dunes of Ashdod-Nizanim, Israel, 1945–1999. J Arid Environ 58(3):335–355

Li ZW, Wang ZY, Brierley G, Nicoll T, Pan BZ, Li YF (2015) Shrinkage of the Ruoergai swamp and changes to landscape connectivity, Qinghai–Tibet Plateau. Catena 126:155–163

Liu LY, Shi PJ, Zou XY, Gao SY, Hasi E, Yan P, Li XY, Dong ZB, Wang JH (2003) Short-term dynamics of wind erosion of three newly cultivated grassland soils in Northern China. Geoderma 115(1–2):55–64

Luo TX, Li WH, Luo J, Wang QJ (1999) A comparative study on biological production of major vegetation types on the Tibetan Plateau. Acta Ecologica Sinica 19(6):823–831 **(In Chinese with English summary)**

Matthews JA, Seppälä M (2014) Holocene environmental change in subarctic aeolian dune fields: the chronology of sand dune reactivation events in relation to forest fires, palaeosol development and climatic variations in Finnish Lapland. The Holocene 24(2):149–164

McKean RLS, Goble RJ, Mason JB, Swinehart JB, Loope DB (2015) Temporal and spatial variability in dune reactivation across the Nebraska Sand Hills, USA. The Holocene 25(3):523–535

Nickling WG, Wolfe SA (1994) The morphology and origin of Nabkhas, region of Mopti, Mali, West Africa. J Arid Environ 28(1):13–30

Sun JM, Ding ZL (1998) Process and cause of land desertification in Northern East China. Quat Sci 18(2):156–164 **(in Chinese with English summary)**

Sun JM, Ding ZL, Liu TS (1998) Desert distributions during the glacial maximum and climatic optimum: example of China. Episc—Newsmag Int Union Geol Sci 21(1):28–31

Sun HL, Zheng D, Yao CD, Zhang Y (2012) Protection and construction of the national ecological security shelter zone on Tibetan Plateau. Acta Geographica Sinica 67(1):3–12 **(In Chinese with English summary)**

Tong CJ, Wu QB (1996) The effect of climate warming on the Qinghai–Tibet Highway, China. Cold Reg Sci Technol 24(1):101–106

Wang T, Zhu Z, Wu W (2002) Sandy desertification in the north of China. Sci China Ser D Earth Sci 45(1):23–34

Xue X, Guo J, Han B, Sun Q, Liu L (2009) The effect of climate warming and permafrost thaw on desertification in the Qinghai–Tibetan Plateau. Geomorphology 108(3):182–190

Yang M, Wang S, Yao T, Gou X, Lu A, Guo X (2004) Desertification and its relationship with permafrost degradation in Qinghai–Xizang (Tibet) plateau. Cold Reg Sci Technol 39(1):47–53

Yang SQ, Gao WS, Sui P, Chen YQ (2005) Quantitative research on factors of soil desertification in Gonghe basin. Acta Ecologica Sinica 25(12):3181–3187 **(in Chinese with English summary)**

Yang X, Ding Z, Fan X, Zhou Z, Ma N (2007) Processes and mechanisms of desertification in northern China during the last 30 years, with a special reference to the Hunshandake Sandy Land, eastern Inner Mongolia. Catena 71(1):2–12

Zhang CL, Dong GR, Zou XY, Cheng H, Yang S (2005) Contributing ratios of several factors to the steppe desertification in Guinan, Qinghai Province. J Desert Res 25(4):511–518 **(in Chinese with English summary)**

Zhou HK, Zhao XQ, Tang YH, Gu S, Zhou L (2005) Alpine grassland degradation and its control in the source region of the Yangtze and Yellow Rivers, China. Grassl Sci 51(3):191–203